Chaos, Solitons & Fractals: X 13 (2024) 100122

Contents lists available at ScienceDirect

Chaos, Solitons & Fractals: X

journal homepage: www.elsevier.com/locate/csfx

Effects of synapse location, delay and background stochastic activity on synchronising hippocampal CA1 neurons

Alessandro Fiasconaro [a,b,c,*], Michele Migliore [c]

[a] Dpto. de Física de la Materia Condensada, Universidad de Zaragoza, 50009 Zaragoza, Spain
[b] Instituto de Biocomputación y Física de Sistemas Complejos, Universidad de Zaragoza, 50018 Zaragoza, Spain
[c] Istituto di Biofisica, Consiglio Nazionale delle Ricerche, Palermo, Italy

ARTICLE INFO

Keywords:
Stochastic modelling
Fluctuation phenomena
Single neuron modelling
Neural systems

ABSTRACT

We study the synchronisation of neurons in a realistic model under the Hodgkin–Huxley dynamics. To focus on the role of the different locations of the excitatory synapses, we use two identical neurons where the set of input signals is grouped at two different distances from the soma. The system is intended to represent a CA1 hippocampal neuron in which the synapses arriving from the CA3 neurons of the trisynaptic pathway appear to be localised in the apical dendritic region and are, in principle, either proximal or distal to the soma. Synchronisation is studied using a specifically defined spiking correlation function as a function of various parameters such as the distance from the soma of one of the synaptic groups, the inhibition weight and the associated activation delay. We found that the neurons' spiking activity depends nonmonotonically on the relative dendritic location of the synapses and their inhibition weight, while the synchronisation measure always decreases with inhibition, and strongly depends on its activation time delay. In our model, the synaptic random subthreshold background activity substantially reduces synchronisation in a monotonic way, while highlights the importance of a balanced E/I contribution for neuronal synchronisation.

Introduction

The mammalian hippocampus, located in the allocortex, is responsible for both short-term and long-term memory. It is the primary area affected in Alzheimer's disease and therefore plays an important role in cognitive function.

The CA1 pyramidal neurons receive two different sets of inputs: one coming directly from the entorhinal cortex (the so-called *perforant path*) and the other from the CA3 neurons, which receive the signal from the granule cells, which in turn receive the signals from the entorhinal cortex (the *trisynaptic path*, so called because three sets of synapses are needed to complete this path).

Much of the brain's function is related to the synchronisation of incoming signals that ultimately lead to an appropriate output [1–4]. Modelling the overlapping contributions in the depolarising membrane potential is therefore of great importance for understanding brain function and for developing theoretical approaches to its malfunctioning.

A large number of papers have investigated the possibility of synchronisation for a large scale of networks using different models. From Kuramoto oscillators [5,6], the Izhikevich model [7], the integrated-and-fire (LIF) schemes [8], with its various generalisations [9–11], or by using the Hodgkin–Huxley (HH) formalism [12], as is the case here.

An overview on synchronisation in the context of basic HH oscillators is given in the works by Boccaletti et al. [13,14], where two-neuron systems, as well as larger network oscillators, are presented.

These modelling efforts have been elucidating many interesting synchronisation scenarios and developed a broad understanding of the synchronisation phenomenon. However, many of these approaches appear limited in different aspects: some of these models represent the neurons as single dynamic dots without internal structure. This approach therefore does not take into account the energy loss due to internal resistance, nor the delays due to the propagation of the current within the neurons. Moreover, this kind of models do not present a relationship between their kinetic parameters and the biological magnitudes involved in neuron functioning. Thus, besides the important basic knowledge it can provide on synchronisation phenomena, this mesoscopic approach neither bridges the gap between physical dynamics and biochemical understanding of the process, nor can it enter into possible medical treatments due to the lack of clear microscopic links between the model parameters and the biological magnitudes (such as synaptic conductances, rise/decay times, signal propagation) that are modified by therapeutic treatments.

* Corresponding author.
E-mail addresses: afiascon@unizar.es (A. Fiasconaro), michele.migliore@cnr.it (M. Migliore).

https://doi.org/10.1016/j.csfx.2024.100122
Received 16 April 2024; Received in revised form 21 October 2024; Accepted 25 October 2024
Available online 4 November 2024
2590-0544/© 2024 The Authors. Published by Elsevier Ltd. This is an open access article under the CC BY-NC-ND license (http://creativecommons.org/licenses/by-nc-nd/4.0/).

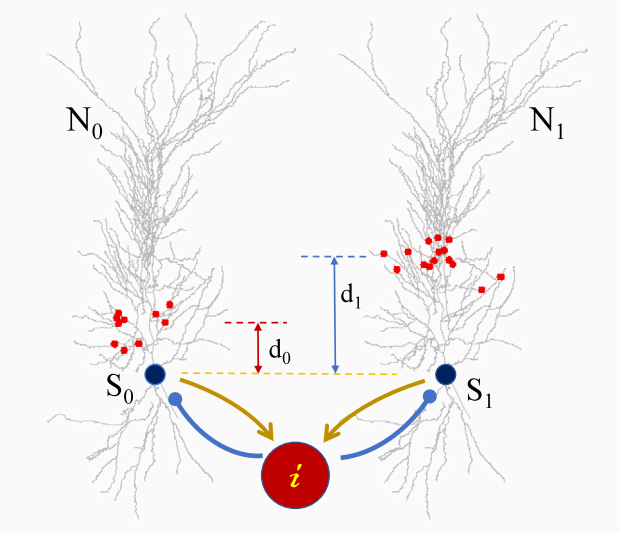

Fig. 1. Scheme of the two identical CA1 neurons, specifically the neuron labelled mpg141017_a1-2_idC [17], that receive inputs from the synapses (red dots in the figure) randomly distributed at different distances from the soma along the apical dendrites. The left neuron N_0 receives the closer synapse distribution (d_0) to the soma, whilst the right one (N_1) receives the synapses in a more distal region (d_1). The model includes an interneuron (i) which, activated by the somas spiking, acts in inhibiting both neuron activity.

As regards the former case – point-like models – it is evident that the different – and stochastic – distribution of excitatory synapses in real neurons makes the spiking process a complex mechanism involving the electrodynamics of pulse propagation along the dendrites, complicated by their shape and geometry [15], or the channel types and their distribution along the dendrites [16]. All of these mechanisms generate non trivial phase shifts in the signals arriving at the somas.

In this context, the present work analyses the possibility of synchronisation of the CA1 spikes generated in response to inputs arriving from CA3 neurons, through synapses distributed at two different distances from the CA1 soma.

Synchronisation is studied for different biological parameters such as the distance of synapses from the soma, the contribution of inhibitory interneurons, the delay of the inhibition, and the activation delay of the proximal synapstic distribution. The excitatory synaptic currents considered here are of the AMPA type, implemented with a double exponential time course with a fast rise and decay time; they are ubiquitous in all neurons.

In addition, the analysis takes into account the background activity on the somas to naively account for large network contributions, as seen in *in vivo* neural cells.

To this end, we apply HH dynamics to two identical neurons subjected to identical Poisson inputs that activate all synapses at the two sets of distances considered. We study synchronisation by a newly defined measure for spiking correlation, using the concept of phase difference between successive spikes.

The article is organised as follows: In Section 1, we provide an explanation of the model, along with the correlation measure defined to assess the synchronisation between spikes. Section 2 contains the main results for the parameters considered, and Section 3 analyses the background contribution to the somas. The paper concludes with some final considerations in Section 4.

1. Methods

The idea is to study the spiking activity on the CA1 neurons, when the signals arrive from two different paths. To do this, we use two identical neurons and generate over them the input as provided by synapses located at two different group positions. The spikes are generated as input pulses with a Poisson time distribution. The source – unique for the two neurons – is connected to the target by means of $N_{syn} = 20$ synapses, that are randomly distributed at a certain mean distance from the soma and varying in each numerical experiment. The chosen N_{syn} represents a reasonable number of active synapses at a given time [18].

Fig. 1 shows two identical realistic and optimised neurons (see [17]) receiving their inputs from the same axon coming from the CA1 neurons of the trisynaptic path. The synapses considered here are AMPA-mediated. This means that their rising current responses are fast, as is their decay time. Moreover, the position of the synapses is not arbitrary. The incoming synapses are located in the apical dendritic area, with a random distribution with a mean value close to the soma in neuron N_0, and with a greater distance from the soma in neuron N_1 (see Ref. [19] for a review on hippocampal neuron morphology).

1.1. Equations and model details

The microscopic neuron dynamics is based on the Hodgkin–Huxley formalism, and the set of equations has been implemented in the NEURON simulation environment [20].

The HH equations are based on the electrodynamics of the neuron membrane and gates, which are characterised by a specific excitability that is reflected in their conductances.

In order to refresh the main mathematics involved in this paper, we briefly outline the original equations. The membrane potential of the neuron at any given membrane segment j can be described by the HH-like equations as follows.

$$C_m \dot{V}_j = I_j^{ext} - I_j^m - I_j^{syn}, \tag{1}$$

where I^{ext} is the external current applied to the gate in the membrane area (in this work this current is always zero), I^m is the membrane current generated in the membrane, and I^{syn} is the postsynaptic current due to the signal received by the incoming synapses. The membrane current has been described schematically by HH as

$$I_j^m = g_{Na} m^3 h (V_j - V_{Na}) + g_K n^4 (V_j - V_K) + g_L (V_j - V_L), \tag{2}$$

where g_a (a = Na, K, L) represent the maximum conductance for sodium, potassium and passive channel (L) ionic currents, respectively, while V_as are the equilibrium potentials of the corresponding channels. The *gating variables* m, h, and n represent the activation/inactivation ratio of the sodium channels and the activation of the potassium channels, respectively.

The ion channels considered are voltage-gated and their opening follows the differential equation

$$\tau_q(V) \frac{dq}{dt} = q_\infty(V) - q. \tag{3}$$

with q representing a generic gating variable; the time function can be expressed as $\tau_q(V) = \frac{1}{\alpha_q(V)+\beta_q(V)}$, and $z_\infty(V) = \frac{\alpha_q(V)}{\alpha_q(V)+\beta_q(V)}$ where the rates α_q and β_q are fitted from experimental data in a sigmoidal fashion due to their underlying kinetic reaction [21].

Beside this simple summary of the equations, the realistic model explored here imposes a more complex set of equations than Eq. (2). In fact, this study considers an extended number of channels that takes into account the experimentally known features of CA1 pyramidal cells, as discussed in recent papers on hippocampal neurons [22,23], against which the configuration and distribution of channels have been thoroughly validated. The complete set of active membrane properties includes the essential sodium current (Na), four types of potassium (K_{DR}, K_A, K_M, and K_D), three types of calcium (CaN, CaL, CaT), the nonspecific I_h current, and two types of Ca-dependent K^+ currents, K_{Ca} and C_{agk}.

With all these contributions, the membrane current term of Eq. (2) modifies in

$$I_{\rm j}^{\rm m} = \sum_a g_a f_a(m,h,n)(V_{\rm j} - V_a), \tag{4}$$

where the sum is extended over all the channels considered, g_a is the maximum conductance, f_a the gating variable, $V_{\rm j}$ the membrane potential and V_a the reversal potential for the channel a, where a= (Na, K_{DR}, K_A, K_M, K_D, CaN, CaL, CaT, I_h, K_{Ca}, C_{agk}). More details on the specific shape of the functions $f_{\rm a}$ and the values of $g_{\rm a}$ can be found in Ref. [22].

All dendritic compartments contain a uniform distribution of channels, except for K_A and I_h which are known to increase linearly with the distance from the soma [24,25] in pyramidal cells. The values for the peak conductance of each channel were optimised independently in each type of neuronal compartment (soma, axon, basal and apical dendrites), with a difference of one order of magnitude [17].

Concerning the postsynaptic current $I^{\rm syn}$, this is modelled for each synapse as [21]

$$I_{\rm j}^{\rm syn} = -g_{\rm syn}\alpha(t - t_{\rm spk} - \tau_{\rm spk})(V_{\rm j} - E_0), \tag{5}$$

with $g_{\rm syn}$ the maximum synaptic conductance. The rate is a double exponential $\alpha(t) = \frac{1}{\tau_{\rm d}-\tau_{\rm r}}(e^{-t/\tau_d} - e^{-t/\tau_r})$, where the mean rise time $\tau_{\rm r}$ and the decay time $\tau_{\rm d}$ are immediately recognised, and the time is reset after each spike ($t_{\rm spk}$), while $\tau_{\rm spk}$ represents a refractory period in which the neuron remains insensitive. E_0 is the synaptic reversal potential, that takes the values $E_0 = 0$ mV in excitatory synapses, and $E_0 = -80$ mV in inhibitory ones. The different reversal potentials are responsible for the sign change of the current induced by the two types of synapses in the dendritic membranes, thus allowing the inhibitory synapses – activated with a suitable physiological delay after the arrival of the stimulus in the circuit – to act as fast attenuators of the membrane potential generated by the excitatory synapses. In this way, the contribution of the inhibitory synapses plays a crucial role in the possibility that the propagation of the signal can generate a depolarisation in the soma.

Our simulations use $\tau_{\rm r} = 3$ ms, and $\tau_{\rm d} = 5$ ms, which makes our excitatory synapses of fast AMPA-mediated type [26], while the inhibition rate is modelled as a single exponential with decay time $\tau_{\rm I,d} = 30$ ms.

The presynaptic Poisson source is generated with a mean frequency $f_{\rm inp} = 60$ Hz corresponding to a gamma brain activity. The two groups of synapses are located as follows: the proximal ones at a fixed mean distance $d_0 = 100\,\mu$m from the soma on neuron N_0, and the other on N_1 at a variable distance $d_1 \in [100, 300]\,\mu$m. The conductance weights of the $N_{\rm syn}$ excitatory synapses are assumed to have the same value $sw = 5 \times 10^{-4}$ nS, while the weight of the inhibitory synapses is in the range $iw \in [0, 0.06]$ nS.

To reduce the fluctuations of our outcomes, the results of our simulations have been averaged over $N_{\rm exp} = 100$ realisations.

1.2. Phase synchronisation

The correlation between spikes in the two neurons is studied by means of the measure c, which modifies an equivalent measure already presented in [27]. The idea is to define the phase of a spiking neuron as [28]:

$$\phi_{\rm i}(t) = 2\pi\frac{t - t_{\rm k}}{t_{\rm k+1,i} - t_{\rm k,i}}, \tag{6}$$

where the index $i = 0, 1$ indicates the neuron N_i, and the time $t_{\rm k,i}$ is the time of the kth spike of N_i. Thus, at time t, the neuron lies at a certain fraction of the total time between two successive spikes, the latter covering a phase spanning between 0 and 2π. This allows us to define the time average of the cosine of the phase difference between the two neurons in a single trace j as

$$c_{\rm j} = \frac{1}{t_{\rm fin} - t_{\rm in}}\int_{t_{\rm in}}^{t_{\rm fin}} \cos(\phi_1(t) - \phi_0(t))\,dt, \tag{7}$$

where $t_{\rm fin} - t_{\rm in}$ defines the maximum window used for the time average in which the phase results well-defined for both neurons. This measure is normalised in the interval $[-1, 1]$, where the value -1 represents the anti-correlated spiking (phase difference equal to π) and the full correlation is given by $+1$ (phase difference 0). The random distribution of the phases is then revealed by the correlation value $c_{\rm j} = 0$ (mean phase difference $\pi/2$).

Given the stochastic nature of the spiking, this measure is then averaged over the number of simulated realisations $N_{\rm exp}$:

$$\langle C_{\rm R}\rangle = \frac{1}{N_{\rm exp}}\sum_{j=1}^{N_{\rm exp}} c_{\rm j}, \tag{8}$$

This spiking synchronisation measure, or others of the same kind, can be generalised for neuron synchronisation in large networks [27], although other options are also used for pairwise correlations [29].

The models studied here is fully available in the ModelDB public database, accession number 2018009 (https://modeldb.science/2018009).

2. Results

Fig. 2 shows the frequency response of the two neurons ν_0 and ν_1 (panels (a) and (b)) under a frequency input $f_{\rm inp} = 60$ Hz as a function of the distance d_1 for different inhibitory weights iw. We observe a weak variation of ν_0 as a function of d_1, with a nonmonotonic trend. Surprisingly, although the spiking activity decreases for increasing values of the iw parameter, we note an increase for increasing distances d_1 with a saturating trend. This means that the further away the second set of synapses is from the soma, the smaller tends to be their effect on N_0. These behaviours show how rich the spiking phenomenon can be when considering realistic neuronal morphologies, and how relevant the role of the interneuron is in mediating the interaction between pyramidal neurons.

An interesting result is the slight increase in spiking activity for the neuron N_1 with increasing distance d_1. In fact, panel (*b*) shows an increase in ν_1 up to a distance of $d_1^* = 150\,\mu$m. For larger distances, the spiking activity of N_1 tends to decrease with a non-monotonic behaviour, probably due to the highly structured dendritic distribution of the realistic neuron. We also note that around the same distance value d_1^*, the spiking activity of the two neurons inverts in intensity, as seen in the negative value of the $\nu_1 - \nu_0$ magnitude (panel d), for $d_1 > d_1^*$. The sawtooth behaviour of the plots in Fig. 2(b–d) depends on the specific morphology used for all simulations, as confirmed by simulations carried out by using a different reconstruction (see Fig. A1 in the Appendix).

The phase spiking correlation $\langle C_{\rm R}\rangle$ presented in panel (e) presents a monotonic decrease as a function of both d_1 and the inhibition weight iw (see Fig. 3). This result seems quite natural, given that signals generated in more distal synapses (in N_1) arrive the soma with reduced amplitude and smoothed over a wider time envelope, and consequently may lead to a decrease in spiking correlation.

To better visualise these results, Fig. 3 presents the same calculations as Fig. 2, replotted as a function of the inhibition weight iw. The frequency response of both neurons (panels (a) and (b)) as well as their average (panel (c)) show a clear non-monotonic behaviour of the spiking frequency, with a minimum of ν_0 around $iw^* \approx 0.04$ nS, corresponding to about 40 active inhibitory synapses.

Surprisingly, the synchronisation parameter $\langle C_{\rm R}\rangle$ appears to decrease monotonically with iw, and does not reflect the non-monotonic behaviour evident in the mean spiking frequencies. This result seems to contradict the well-known fact that a small amount of inhibition improves the spiking synchronisation between neurons [30,31], and the issue has been addressed in a paper by Fiasconaro and Migliore [32], where a series of calculations with realistic neurons showed that, under a stochastic current source, an increase in synchronisation is obtained

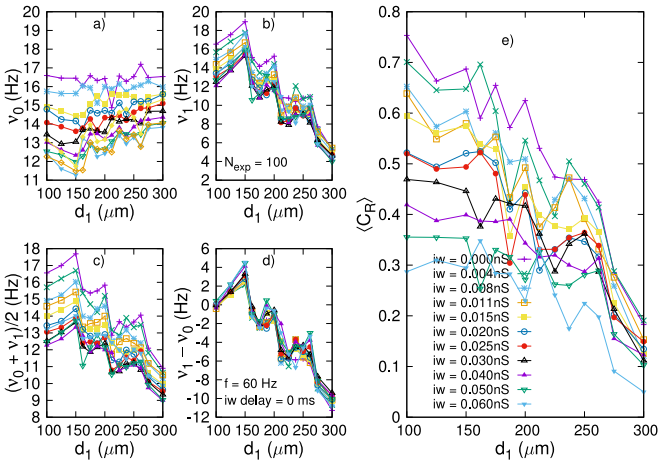

Fig. 2. Frequency response of the two neurons ν_0 (panel a) and ν_1 (panel b) to the Poissonian input at the average frequency $f_{inp} = 60$ Hz as a function of the distance d_1 of the synapses from the soma in neuron N_1. Panel (c) shows the mean frequency between the two neurons, and Panel (d) shows their difference. The spiking correlation (Panel (e)) shows a monotonic decrease with d_1.

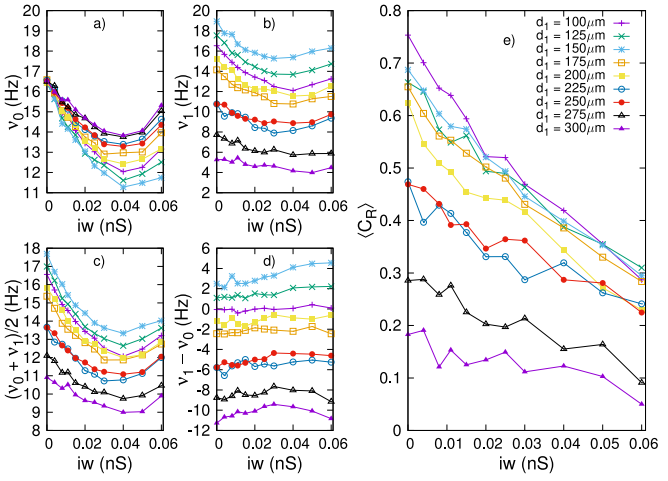

Fig. 3. Frequency response equivalent to the one shown in Fig. 2, shown as a function of the inhibitory weight iw. The delay in the inhibition response is here 0 ms.

with inhibition, provided that the inactivation times of the excitatory synapses τ_d are long enough. This is not the case in this study, since $\tau_d < \tau_{I,d}$.

Fig. 4 shows the spiking traces corresponding to the three cases: $iw = 0, 0.04$, and 0.06 nS. Here we can see another counterintuitive and interesting phenomenon, i.e. the anticipation of the neuron spiking with signal from distal synapses with respect to those arriving from the proximal ones. In fact, the spikes shown in the time window are characterised by the occasional anticipation of the spikes in S_1, with synapse distribution at $d_1 = 150\,\mu$m, compared to the spikes of S_0, with more proximal synapses at $d_0 = 100\,\mu$m (see $iw = 0$ at about 500 ms, and $iw = 0.06$ ns at about 950 ms). This behaviour depends on the fact that distal dendrites are narrower than proximal ones, and it has been demonstrated that the depolarising propagation is better and more efficient there than in wider dendrites [33]. In fact, the rebound of the current at the dendritic terminal tips can allow an overlapping and integration of ion currents inside the dendrite that can more intensely and efficiently stimulate a spiking arrival to the soma, even anticipating its depolarisation. This phenomenon can also increase the overall spiking frequency, thus explaining the increase in the frequency response ν_1 for $d_1 < d_1^*$ shown in Fig. 2(b).

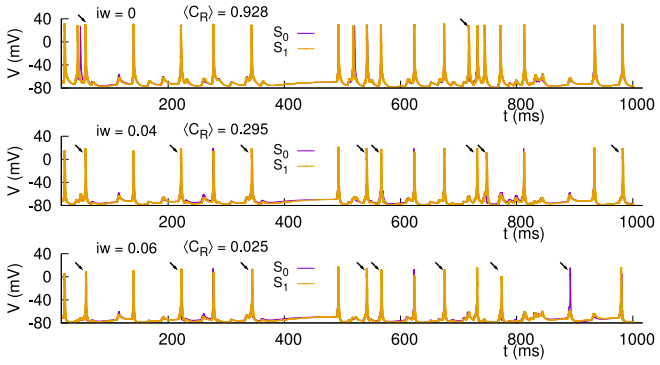

Fig. 4. Time evolution of the spiking activity in the two neurons with different average synapse locations ($d_0 = 100$ and $d_1 = 150\,\mu$m) at $f_{inp} = 60$ Hz for $iw = 0, 0.04, 0.06$ nS. It is evident that there is an occasional anticipation of soma spikes in S_1 compared to S_0 (top panel at 500 ms, and bottom panel at 950 ms), and a decrease in frequency response as iw increases, also due to spiking failures. The tiny arrows indicate the spikes occurring only in one of the two somas.

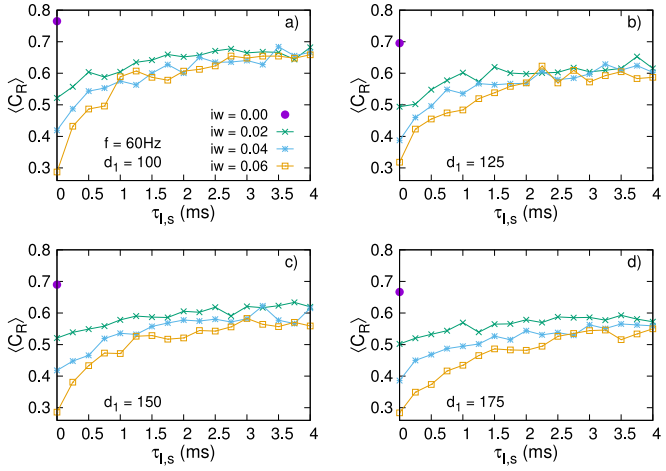

Fig. 5. Spiking correlation is shown as a function of the synapse inhibitory delay $\tau_{I,s}$ for various values of the inhibitory weight, specifically $iw = 0, 0.02, 0.04, 0.06$ nS. The panels refer to different mean distances from the soma of N_1, $d_1 = 100, 125, 150, 175\,\mu$m. The presence of inhibition ($iw \neq 0$) reduces the spiking synchronisation $\langle C_R\rangle$ in comparison to the uninhibited values (represented by a full circle in the plots). For inhibited dynamics, $\langle C_R\rangle$ increases monotonically with a saturating trend, almost reaching the uninhibited value.

Fig. 4 also evidences the non-monotonic response frequency when increasing the inhibition weight iw, and the larger difference in S_0 (blue line) compared to S_1. Moreover, the spiking response when increasing the inhibitory weight is accompanied by more frequent spiking failures in S_0 than in S_1.

To better understand the role of some time delays in CA1 synchronisation, we performed a series of calculations by changing the synaptic inhibition delay $\tau_{I,s}$, i.e. the delay used by the interneurons to respond and inhibit both neurons. Fig. 5 shows the phase spiking correlation $\langle C_R\rangle$ as a function of the synaptic delay $\tau_{I,s}$ in the inhibition of interneuron activation by the soma spiking. The inhibition works with both a forward and backward mechanism, because, regardless of which neuron spikes, the interneurons act on both neurons at the same time (see the graph in Fig. 1).

The interneuron has not been explicitly implemented in the network, but it was modelled as an inhibitory synaptic current according to Eq. (5). To implement a plausible signal propagation in the circuit, we introduced a delay for its activation, with respect to the action potential in the presynaptic pyramidal cell.

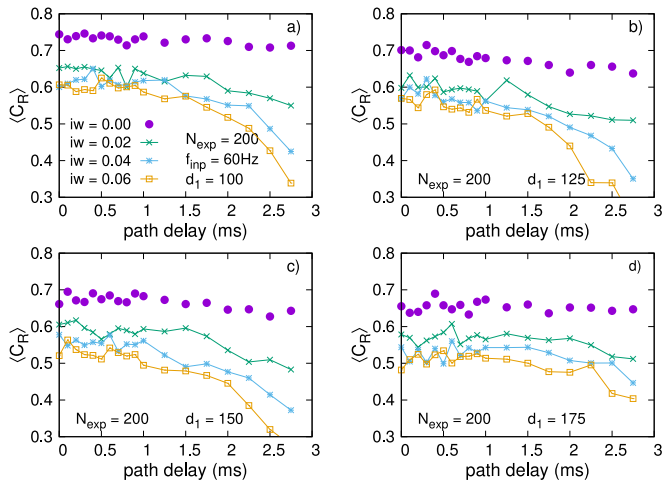

Fig. 6. Spiking correlation as a function of the *path delay* $\tau_{E,del}$ for different inhibition weights and different distances d_1 from the soma. Synchronisation appears weakly affected up to values of $\tau_{E,del} \approx 2$ ms. The inhibition delay here is $\tau_{I,s} = 2$ ms.

The plots indicate that the presence of inhibition decreases the synchronisation features. In fact, all the curves (with $iw = 0.01, 0.02, 0.05$ nS) are below the full points in the figures, which represents the absence of inhibition ($iw = 0$ nS). Specifically, the absence of delay represents the maximum loss of synchronisation, while for increasing values of $\tau_{I,s}$ a saturating increase in synchronisation is reported. The same behaviour is confirmed for all the distances from the soma in the neuron N_1 shown in the three panels of Fig. 5, specifically $d_1 = 100\,\mu$m, i.e. no mean distance between the synaptic location of the two neurons, $d_1 = 150\,\mu$m and $d_1 = 200\,\mu$m. The difference in the three distances only reflects the expectable outcome that by increasing the distance d_1, the synchronisation decreases, as shown in Fig. 2.

In order to investigate whether and to what extent a difference in the activation times of the CA3 afferent volleys can affect synchronisation, a series of simulations have been run in which the excitatory inputs to the proximal set of synapses was delayed by a few milliseconds with respect to the distal set. This *path delay* ($\tau_{E,del}$) has been applied to the synaptic activation time of the N_0 neuron synapses, and allowed to study the details of their optimal integration with the signal generated by the distal inputs and propagating towards the soma.

Fig. 6 shows the spiking correlation $\langle C_R \rangle$ as a function of this delay for four inhibition weights (iw =0, 0.01, 0.02 and 0.05 nS) and four distances of the second neuron from the soma: $d_1 = 100, 125, 150, 175\,\mu$m. We can observe here that no significant contribution is due to the excitatory delay $\tau_{E,del}$ in synchronising the signals for the different inhibition weights studied. In fact, although for all the distances the curves with $iw \neq 0$ lie below the full blue dots indicating the correlation with no inhibition, those curves seem to remain essentially unchanged for low time delays ($\tau_{E,del} \lesssim 1.5$ ms), time at which a fast synchronisation decay occurs. This calculation confirms that the presented model predicts that the regulatory function of the interneurons with their inhibitory activity on the CA1 neurons barely affects AMPA-mediated synapses.

3. Stochastic background contribution

The model described above has been analysed here with the two neurons disconnected from the brain network, only connected to the incoming signals modelled as a Poisson process activating the excitatory synapses. In order to better understand a more complex and realistic scenario, we have carried out a series of calculations in which, maintaining the distributed synapses already investigated in the previous section, the two somas are reached by a noisy background, with the aim of representing in a simple way the stochastic contribution provided by the many connections of the brain networks on the activity of the two neurons studied here, thus reproducing a *in vivo*-like activity. This contribution follows the Destexhe approach [34,35], where two synapses, one excitatory and the other inhibitory, are both characterised by a mean value of the maximum conductances $g_{OU,x}$ together with an additional stochastic term. The latter is modelled as an Ornstein–Uhlenbeck (OU) fluctuation with a given noise intensity σ_x and a correlation time $\tau_{OU,x}$, where the suffix x indicates the two possibilities: $x = E$ or $x = I$ for the excitatory or inhibitory synapse, respectively. Using this "fluctuating conductance approach", they were able to successfully simulate a neocortical neuron response that reproduced a typical experimental trace, under simpler conditions than those presented in this paper.

The equation added to the system is then the two-term contribution to the current

$$I^{stoch} = g_{OU,E}(t)(V - E_E) + g_{OU,I}(t)(V - E_I), \tag{9}$$

with reversal potential $E_E = 0$ and $E_I = -80$, values similar to the distributed synapses. The maximum conductances follow independently of each other an Ornstein–Uhlenbeck process:

$$\frac{dg_{OU,x}(t)}{dt} = \frac{1}{\tau_{OU,x}}[g_{OU,x} - g_x] + \sqrt{2\sigma_x}\eta_x(t), \tag{10}$$

where g_x are the average maximum conductances of the added synapses, $\tau_{OU,x}$ is the correlation time of the OU process, σ_x is the intensity of the fluctuations, and $\eta_x(t)$ is the zero mean uncorrelated Gaussian noise ($\langle \eta_x(t) \rangle = 0$ and correlation $\langle \eta_x(t)\eta_y(t') \rangle = \delta(t - t')$). See [35,36] for further details on the updating rules for numerical integration of the above equations.

We carried out three different sets of calculations. In the first, we spanned only some conductance values and corresponding noise intensities with the excitatory term, excluding the inhibitory contribution. In the second, we only spanned the inhibitory term, again in terms of mean conductance and fluctuation intensity, excluding the excitatory contributions. In the third one, we spanned the combined contributions of inhibition and excitation, fixing the value of the two corresponding fluctuation intensities to the value of the maxima registered in the previous cases. The OU time correlations have been fixed to the values $\tau_{OU,E} = 3$ ms in the case of excitatory synapses, and to the value $\tau_{OU,I} = 10$ ms in the case of inhibitory ones.

Figs. 7, 8 and 9 show the results of the simulations by spanning the two parameters respectively considered and schematised in the panels (a) and (b), which record the output frequencies of the two somas, panel (c) which shows the spiking correlation $\langle C_R \rangle$ and panel (d) which shows the projection of $\langle C_R \rangle$ along one of the parameters in the 3D plots.

In Fig. 7(a) and (b) we can observe how the excitatory-only background activity always increases the average spiking frequency, regardless of the fluctuation intensity. A more structured behaviour is present in panel (c) for the spiking correlation, where $\langle C_R \rangle$ increases with the mean conductance, whilst a clear decrease is observed as a function of the fluctuation intensities σ_E, the latter results more visible in panel (d) for some values of the mean maximum conductance g_E.

More interesting is the response of the neurons to the inhibitory background activity. We can see in Fig. 8 that, besides the expected monotonic decrease of the output spiking frequencies in both neurons with the average inhibition weight g_I, the spiking correlation reveals a non-monotonic behaviour with g_I (see panel (c)) with a clear maximum that also depends on the noise intensity. Panel (d) shows the correlation $\langle C_R \rangle$ as a function of the average inhibitory weight g_I for three fluctuation intensities, showing a clear maximum with a relative increase with respect to the previous minimum of about $\approx 10\%$. Instead, the correlation decreases monotonically with the noise intensity. Finally, the third set of calculations has been performed with fixed noise intensities in both cases (excitatory and inhibitory). Specifically we

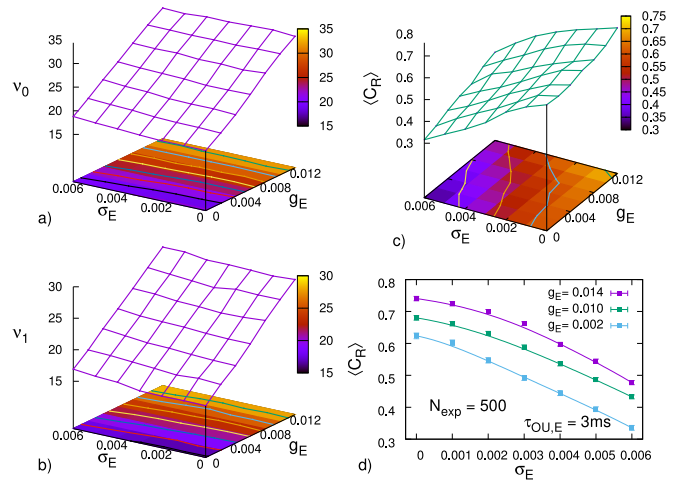

Fig. 7. Spiking correlation as a function of the excitatory fluctuating conductance parameters: the average conductance g_E and noise intensity σ_E. The OU correlation time is $\tau_{OU,E} = 3$ ms in this case. The parameters for the distributed synapses in this plot are $iw = 0.01$ nS, $d_1 = 175\,\mu$m, and $\tau_d = 5$ ms. The excitatory fluctuating term decreases monotonically the spiking correlation $\langle C_R \rangle$.

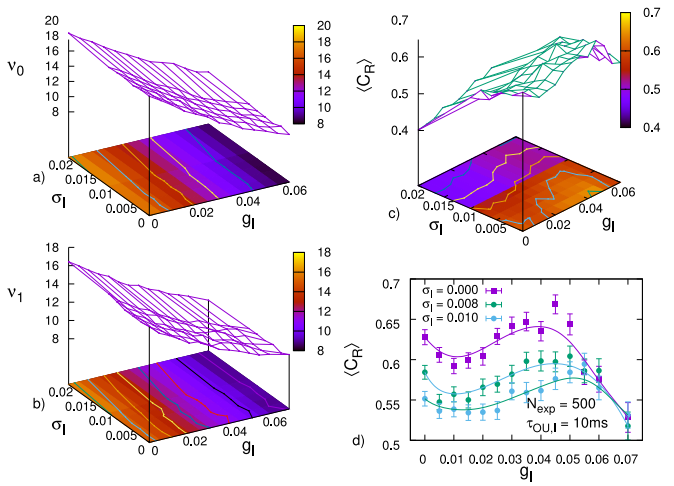

Fig. 8. Spiking correlation as a function of the inhibitory fluctuating conductance parameters: average $g_{OU,I}$ and noise intensity σ_I. The OU correlation time is here $\tau_{OU,I} = 10$ ms. The parameters of the distributed synapses are the same as Fig. 7.

have chosen the maximum values of the calculations performed above, i.e. $\sigma_E = 0$ and $\sigma_I = 0$, but similar behaviour is recovered with non-zero noise intensities. This mixture of excitation and inhibition reveals a clear non-monotonic behaviour of the spiking correlation as a function of both magnitudes g_E and g_I, with optimal correlations for a proper g_I-g_E combination, as seen in Fig. 9(c). Panel (d) shows a selection of $\langle C_R \rangle$ curves as a function of the g_I for three values of the background excitatory weight g_E, where this complex behaviour of the two measures appears. The balance between excitation and inhibition is an important neurophysiological factor. In fact, the absence of inhibition leads to epileptic activity [37] and loss of sensory selectivity [38]. Some estimates of the weight of the two conductances have been made using data from cortical neurons [39,40], and fitting the output with a LIF model [41], a 4 to 1 ratio between inhibitory/excitatory conductances was calculated. In another case, during slow-wave sleep activity and in depolarised conditions (up-phase), excitatory and inhibitory synaptic conductances are balanced with a ratio of 1 [42,43], whereas in the awake state inhibition becomes predominant [44]. In the presented model, the inhibitory background activity provides optimal synchronisation conditions at values about one order of magnitude higher than the excitatory ones.

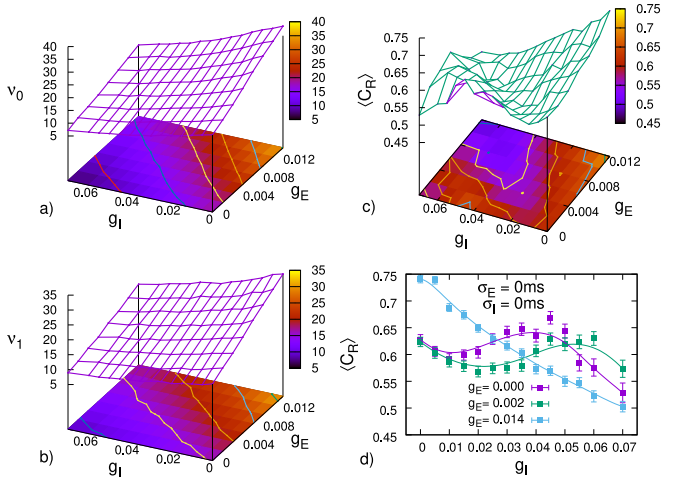

Fig. 9. Spiking correlation as a function of both excitatory and inhibitory background conductances in the OU scheme: The parameters of the distributed synapses are the same as Figs. 7 and 8.

4. Summary and conclusions

We have studied the synchronisation behaviour of two CA1 neurons subjected to Poissonian inputs at a frequency $f_{inp} = 60$ Hz as a function of the different distances from the soma of the excitatory synapses arriving from the CA3 neurons of the Hippocampus trisynaptic path.

The spiking activity in the two neurons appears nonmonotonic with the distance of the synapse distribution in the second neuron, with a extremal value at d_1^*, which is a minimum value for the neuron with the synapse distribution at d_0 (see Fig. 2(a)), and a maximum value for N_1 with distal synapses (Fig. 2(c)), showing the counterintuitive effect of increasing spiking frequency for distal synapses.

The spiking activity of both neurons decreases nonmonotonically with the inhibitory weight, with a minimum value corresponding to about 40 active interneurons (Fig. 3).

Regarding the synchronisation properties measured by the phase spiking correlation $\langle C_R \rangle$ we always observe a decrease with the weight of the inhibitory synapses, as well as with the distance of the synapse distribution (Figs. 2 and 3). Moreover, in the limit of small distances ($d_1 \lesssim 200\,\mu$m), synchronisation is weakly influenced by the path time delays in the excitatory synapses $\tau_{E,del}$ if they remain at low values ($\tau_{E,del} \lesssim 2$ ms) (see Fig. 6). The absence of an increase in synchronisation with the inhibition is essentially due to the short time decay of the AMPA synapses for which the inhibition plays no constructive role. Nevertheless, we also observe, always in the presence of inhibition, an increase of the phase spiking correlation with the time delay $\tau_{I,s}$ at which the interneurons activate (Fig. 5).

The results presented here show that, in the absence of a stochastic background, the fast AMPA excitatory synapses are not able to increase the synchronisation of soma spiking, even in the presence of the inhibition given by interneurons. The latter simply act as modulators, with nonmonotonic behaviour, of the frequency response of the neurons.

Moreover, the presence of the unavoidable stochastic background in *in vivo* functioning (see Figs. 7 to 9) shows that the fluctuations do not play any constructive role in this model, and that they mainly contribute to reducing the spiking correlation of the system. Instead,

an increase in synchronisation can be achieved by a combined excitatory/inhibitory background activity in the presence of optimal conditions for a range of suitable conductances, with a dominant inhibition weight of about one order of magnitude with respect to excitatory synapses.

CRediT authorship contribution statement

Alessandro Fiasconaro: Writing – review & editing, Writing – original draft, Software, Investigation, Conceptualization. **Michele Migliore:** Writing – original draft, Supervision, Conceptualization.

Declaration of competing interest

The authors declare the following financial interests/personal relationships which may be considered as potential competing interests: Alessandro Fiasconaro reports financial support was provided by European Union Next-GenerationEU. Alessandro Fiasconaro reports financial support was provided by Government of Spain Ministry of Development. Michele Migliore reports financial support was provided by European Union Next-GenerationEU. Alessandro Fiasconaro reports financial support was provided by Government of Aragón. If there are other authors, they declare that they have no known competing financial interests or personal relationships that could have appeared to influence the work reported in this paper.

Acknowledgements

The authors acknowledge the grant PID2020-113582GB-I00 funded by MCIN/AEI/10.13039/501100011033, the grant PID2023-147734NB-I00 funded by MCIN/AEI, the support of the Aragon Government to the Recognized group 'E36_23R Física Estadística y no-lineal (FENOL)'. We also acknowledge a contribution from the Italian National Recovery and Resilience Plan (NRRP), M4C2, funded by the European Union –NextGenerationEU (Project EBRAINS-Italy), and the funds of the European Union NextGenerationEU/PRTR through the spanish Ministerio de Universidades (BOA 139 (31185) 01/07/2021).

Appendix

Fig. 2 shows a clear sawtooth behaviour in panels (b), (c), and (d). This intriguing feature is only due to the specific morphology implemented in our simulations. In order to check out this point, a series of calculations have been performed by using a different realistic morphology, to investigate the analogue outcomes as those reported above.

In particular, the structure used is the one labelled mpg141209_A_idA in Ref. [17]. The results are shown in Fig. 10, equivalent to Fig. 2, where it is evident that the detailed sawtooth behaviour has disappeared, though leaving the main qualitative trend previously encountered. In fact, a global maximum is present for the frequency spiking ν_1 as a function of d_1 (panels (b–d)) around the value $d_1^* \approx 200\,\mu$m, while the other morphology presented it at $d_1^* \approx 150\,\mu$m with a sharper peak. Again, the correlation measure appears monotonic, except for a small increase at the very last value $d_1 = 300\,\mu$m. This example confirms the strong heterogeneity in the spiking details that a specific morphology can produce.

Data availability

No data was used for the research described in the article.

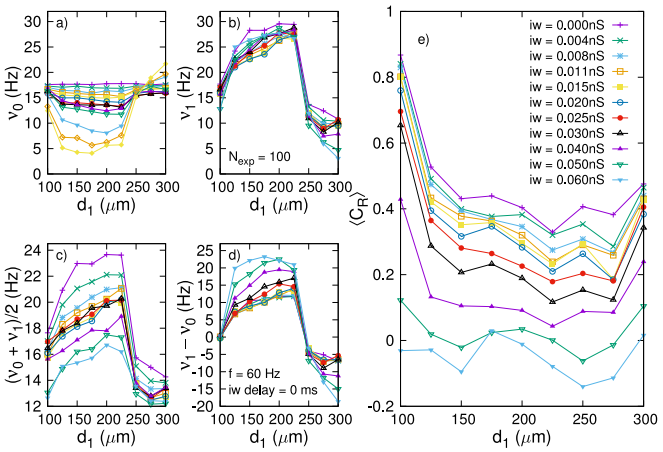

Fig. 10. Frequency response of the two neurons ν_0 (panel a) and ν_1 (panel b) to the Poissonian input at the average frequency $f_{inp} = 60\,$Hz as a function of the distance d_1 of the synapses from the soma in neuron N_1. Panel (c) shows the mean frequency between the two neurons, and panel (d) shows their difference. The spiking correlation is reported in panel (e).

References

[1] Fries P. Rhythms for cognition: Communication through coherence. Neuron 2015;88:220.
[2] J. O'Keefe, Recce ML. Phase relationship between hippocampal place units and the EEG theta rhythm. Hippocampus 1993;3:317.
[3] Mainen ZF, Sejnowski TJ. Reliability of spike timing in neocortical neurons. Science 1995;268:1503.
[4] Hopfield JJ. Pattern recognition computation using action potential timing for stimulus representation. Nature 1995;376:33.
[5] Kuramoto Y. Self-entrainment of a population of coupled nonlinear oscillators. Lecture Notes in Phys 1975;39:420.
[6] Acebrón JA, Bonilla LL, Pérez-Vicente CJ, Ritort F, Spigler R. The kuramoto model: A simple paradigm for synchronisation phenomena. Rev Modern Phys 2005;77:137.
[7] Izhikewich EM. Simple model of spiking neurons. IEEE Trans Neural Netw 2003;14:1569.
[8] Abbott LF. Lapicque's introduction of the integrate-and-fire model neuron (1907). Brain Res Bul 1999;50(5–6):303, 10.1016/S0361-9230(99)00161-6.
[9] Brette R, Gerstner W. Adaptive exponential integrate-and-fire model as an effective description of neuronal activity. J Neurophysiol 2005;94(5):3637. http://dx.doi.org/10.1152/jn.00686.2005.
[10] Górski T, Depannemaecker D, Destexhe A. Conductance-based adaptive exponential integrate-and-fire model. Neural Comput 2021;33(1):41. http://dx.doi.org/10.1162/neco_a_01342.
[11] Marasco A, Spera E, De Falco V, et al. An adaptive generalized leaky integrate-and-fire model for hippocampal CA1 pyramidal neurons and interneurons. Bull Math Biol 2023;85:109, 10.1007/s11538-023-01206-8.
[12] Hodgkin AL, Huxley AF. A quantitative description of membrane current and its application to conduction and excitation in nerve. J Physiol 1952;11:500.
[13] Boccaletti S, Pisarchik AN, del Genio CI, Amann A. Synchronization: From coupled systems to complex networks. Cambridge University Press; 2018.
[14] Boccaletti S, Kurths J, Osipov G, Valladares DL, Zhou CS. The synchronization of chaotic systems. Phys Rep 2002;366:1–101.
[15] Li L, Gervasi N, Girault JA. Dendritic geometry shapes neuronal cAMP signalling to the nucleus. Nature Commun 2015;6:6319.
[16] Migliore M, Sheperd GM. Emerging rules for the distributions of active dendritic conductances. Nature Rev Neurosci 2002;3:362.
[17] Migliore R, Lupascu CA, Bologna LL, Romani A, Courcol J-D, Antonel S, et al. The physiological variability of channel density in hippocampal CA1 pyramidal cells and interneurons explored using a unified data-driven modeling workflow. PLoS Comput Biol 2018;14(9):e1006423. http://dx.doi.org/10.1371/journal.pcbi.1006423.
[18] Megías M, Emri Zs, Freund TF, Gulyás AI. Total number and distribution of inhibitory and excitatory synapses on hippocampal ca1 pyramidal cells. Neuroscience 2001;102(3):527.
[19] Spruston N. Pyramidal neurons: dendritic structure and synaptic integration. Nature Rev Neurosci 2008;9:206–21.
[20] Hines ML, Carnevale NT. The NEURON simulation environment. Neural Comput 1997;9:1179.

[21] Destexhe A, Mainen Z, Sejnowski T. An efficient method for computing synaptic conductances based on a kinetic model of receptor binding. Neural Comput 1994;6:1418.
[22] Ascoli GA, Gasparini S, Medinilla V, Migliore M. Local control of postinhibitory rebound spiking in CA1 pyramidal neuron dendrites. J Neurosci 2010;30:6434.
[23] Morse TM, Carnevale NT, Mutalik PG, Migliore M, Shepherd GM. Abnormal excitability of oblique dendrites implicated in early Alzheimer's: A computational study. Front Neural Circuits 2010;4:16.
[24] Hoffman DA, Johnston D. Neuromodulation of dendritic action potentials. J Neurophysiol 1999;81:408.
[25] Magee JC. Dendritic I_h normalizes temporal summation in hippocampal CA1 neurons. Nature Neurosci 1999;2:508.
[26] Kleppe IC, Robinson HPC. Determining the activation time course of synaptic AMPA receptors from openings of colocalized NMDA receptors. Biophys J 1999;77:1418.
[27] Pérez T, Garcia GC, Eguíluz VM, Vicente R, Pipa G, Mirasso C. Effect of the topology and delayed interactions in neuronal networks synchronisation. PLoS One 2011;6:e19900.
[28] Pikovsky A, Rosenblum M, Osipov G, Kurths J. Phase synchronisation of chaotic oscillators by external driving. Phys D 1997;104:219.
[29] de la Rocha J, Doiron B, Shea-Brown E, Josić K, Alex Reyes A. Correlation between neural spike trains increases with firing rate. Nature 2007;448:802.
[30] Noebels JL, Avoli M, Rogawski MA, Olsen RW, Delgado-Escueta AV. Jasper's basic mechanisms of the epilepsies. fourth ed.. USA: Oxford University Press; 2012.
[31] Bazhenov M, Stopfer M. Forward and back: Motifs of inhibition in olfactory processing. Neuron 2010;167:357.
[32] Fiasconaro A, Migliore M. Hippocampal synchronization in a realistic ca1 neuron model. Phys. Rev. E 2024;110:044406.
[33] Migliore M, Ferrante M, Ascoli GA. Signal propagation in oblique dendrites of CA1 pyramidal cells. J Neurophysiol 2005;94:4145.
[34] Destexhe A, Paré D. Impact of network activity on the integrative properties of neocortical pyramidal neurons *in vivo*. J Neurophysiol 1999;81:1531.
[35] Destexhe A, Rudolph M, Fellous JM, Sejnowski TJ. Fluctuating synaptic conductances recreate *in vivo*-like activity in neocortical neurons. Neuroscience 2001;107:13.
[36] Gillespie DT. The mathematics of Brownian motion and Johnson noise. Am J Phys 1996;64:225.
[37] Dichter MA, Ayala GF. Cellular mechanisms of epilepsy: A status report. Science 1987;237:157.
[38] Sillito AM. The contribution of inhibitory mechanisms to the receptive field properties of neurones in the striate cortex of the cat. J Physiol 1975;250:305.
[39] Borg-Graham LJ, Monier C, Fregnac Y. Voltage-clamp measurement of visually-evoked conductances with whole-cell patch recordings in primary visual cortex. J Physiol Paris 1996;90:185.
[40] Borg-Graham LJ, Monier C, Fregnac Y. Visual input evokes transient and strong shunting inhibition in visual cortical neurons. Nature 1998;393:369.
[41] Monier C, Fournier J, Fregnac Y. In vitro and in vivo measures of evoked excitatory and inhibitory conductance dynamics in sensory cortices. J Neurosci Methods 2008;169:323.
[42] Shu Y, Hasenstaub A, McCormick DA. Turning on and off recurrent balanced cortical activity. Nature 2003;423:288.
[43] Haider B, Duque A, Hasenstaub AR, McCormick DA. Neocortical network activity in vivo is generated through a dynamic balance of excitation and inhibition. J Neurosci 2006;26:4535.
[44] Haider B, Häusser M, Carandini M. Inhibition dominates sensory responses in the awake cortex. Nature 2013;493:97.